A Hierarchical Three-dimensional Porous Laser Scribed Graphene Film for Suppressing Polysulfide Shuttling in Lithium-Sulfur Batteries

Eman Alhajji, [†,1] Wenxi Wang, [†,1] Wenli Zhang,[†] and Husam N. Alshareef[*†]*

[†] *Materials Science and Engineering,* Physical Science and Engineering Division, King Abdullah University of Science and Technology (KAUST), Thuwal 23955-6900, Saudi Arabia

***** E-mail: husam.alshareef@kaust.edu.sa (H.N.A.)

[1] Authors with equal contributions

ABSTRACT

Lithium-sulfur (Li-S) battery is a promising next-generation rechargeable battery with high energy density. Given the outstanding capacities of sulfur (1675 mAh g^{-1}) and lithium metal (3861 mAh g^{-1}), Li-S battery theoretically delivers an ultra-high energy density of 2567 Wh kg^{-1}. However, this energy density cannot be realized due to several factors, particularly the shuttling of polysulfide intermediates between the cathode and anode, which causes serious degradation of capacity and cycling stability of a Li-S battery. In this work, a simple and scalable route was employed to construct a free-standing laser scribed graphene (LSG) interlayer which effectively suppresses the polysulfide shuttling in Li-S batteries. Thus, a high specific capacity (1160 mAh g^{-1}) with excellent cycling stability (80.4% capacity retention after 100 cycles) has been achieved due to the unique structure of hierarchical three-dimensional pores in the free-standing LSG.

KEYWORDS: Laser Scribed Graphene, Graphene, Lithium-sulfur battery, Interlayer, High-capacity, Polysulfide shuttling

1. INTRODUCTION

Today, our society is becoming more and more electrified, which has caused an endlessly aggregating demand for advanced rechargeable batteries.[1] One leading sector is electrical transportation which requires batteries with high energy densities, low self-discharge rates, and long cycling lives. Such requirements are challenging to be met by conventional lithium-ion batteries as they approach their limits.[2] A promising candidate for future researchable batteries is lithium-sulfur (Li-S) battery, a type of lithium-metal energy storage system with high energy density.[3] Besides the appealing advantage of the high theoretical capacity of sulfur, elemental sulfur is non-toxic and can be found abundantly in nature worldwide. Sulfur is also a waste by-product of the petrochemical industry, which ensures the relatively low cost of Li-S batteries.[4]

Attributed to the ultrahigh capacities of sulfur and Li metal (1675 and 3861 mAh g^{-1}, respectively) and an operating voltage of 2.15 V, Li-S battery holds a high theoretical energy density of 2567 Wh kg^{-1}.[5–7] During the discharge process, cyclic-S_8 is converted into a succession of soluble polysulfide intermediates (Li_2S_8, Li_2S_6, and Li_2S_4; 2.4–2.2 V) and eventually insoluble species (Li_2S_2 and Li_2S; 2.2–1.8 V). [8,9] Nonetheless, Li-S batteries suffer from a perilous challenge, the internal migration of the dissolved intermediate lithium polysulfides (LiPSs) between the anode and the cathode. This phenomenon is called the shuttling effect, which significantly decreases the electrochemical capacity of active materials and consequently causes rapid deterioration of the battery performance. [10]

To overcome this challenge, researchers have proposed two different approaches. The first approach was to synthesize novel cathode hosts that physically or chemically confine polysulfides dissolution within the cathode, such as conductive carbon microspheres [11], carbon nanotubes [12],

and reduced graphene oxides [13]. The second approach is to insert an interlayer between the cathode and separator, leveraging an outer design modification.

Since Manthiram's research group first published the concept of "interlayer" in 2012,[14] different carbonaceous, metallic, and polymeric materials have been studied as interlayers, aiming to enhance the electrochemical performances of Li-S batteries to a practical level. [15,16] The most dominant class of the reported interlayers is the carbon-based layers because of its abundance and unique physical and chemical properties, such as low density, high conductivity, and excellent stability. Carbonaceous materials such as biomass-derived carbons[17–19] and graphene-based materials [20–22] were first explored but showed limited progress. To increase the chemical anchoring capability of the interlayers utilized in Li-S batteries, researchers begun to introduce hybrids of carbon materials such as graphene-embedded carbon fiber[23] and free-standing hollow carbon nanofiber on reduced graphene oxide (rGO)[22]. Other studies sightsaw the advantage of heteroatomic doping in increasing the polarity of interlayers. Sulfur-nitrogen dual-doped graphene [24] and nitrogen and phosphorous dual doped graphene [25] are excellent examples of the success of such an approach. Similarly, polar metal oxides such as Fe_3O_4-decorated porous graphene (Fe_3O_4-PG) have been reported to be effective in enhancing the performance of Li-S batteries [26].

Nonetheless, the previously mentioned studies lack the feasibility of fabrication. More specifically, the synthesis of bio-mass derived carbons often requires high thermal carbonization (800 to 1000 ^oC) for several hours, which consumes an intensive amount of energy input.[15,16,25] Likewise, the preparation of rGO, SNGE, p-NP-G, and Fe_3O_4-PG involves a tedious process of chemical exfoliation and filtration in addition to the use of toxic solutions such as sulfuric acid (H_2SO_4).[27]

Laser scribed graphene (LSG) is a type of carbonaceous material derived from polyimide under ambient CO_2 laser irradiation. LSG shows a three-dimensional turbostratic graphitic structure.[28] Since its discovery, LSG has attracted considerable attention in the scientific community due to its high conductivity and high surface area. The merits of LSG endow it with various energy-environmental related applications such as sensors[29], supercapacitors[30], and batteries[31]. Given the three-dimensional architecture, high specific surface area, a wide range of pore size distribution of LSGs, LSG could act as an effective interlayer for inhibiting the shuttling of polysulfides during the charge-discharge of Li-S batteries.

In this paper, we propose a scalable and straightforward route for synthesizing a free-standing laser scribed graphene (LSG) interlayer with unique hierarchical porosity for advanced Li-S batteries, which adds a significant piece to the wide applications reported for LSG. [28,32] Besides simplicity and scalability, the synthesis of LSG is conducted at ambient conditions and involves no toxic solvents, which further promotes the research, development, and commercialization of Li-S batteries.

2. RESULTS AND DISCUSSION

The polysulfide intermediates produced during the discharge process are highly polar and soluble. Nevertheless, most separators used in Li-S batteries are composed of nonpolar macroporous materials such as polypropylene, polyethylene or glass fiber, which cannot confine polysulfides shuttling. Herein, we report a simple and scalable method to fabricate hierarchical porous laser scribed graphene (LSG) as an intercalated layer for Li-S batteries. Figure 1 shows the synthetic scheme for the preparation of a Li-S cell with the LSG interlayer. The LSG composite,

as an interlayer for Li-S battery, has a unique hierarchical porosity, which could adsorb polysulfides species and suppress the shuttling of polysulfides.

LSG was obtained by irradiating CO_2 laser on a commercial Kapton polyimide film under ambient conditions, following the simple direct writing technique published by Tour's group [33]. LSG is a type of three-dimensional polycrystalline carbon with high conductivity and high surface area. These LSG merits endow various electrochemical applications such as sensors [29], supercapacitors [30], and batteries [31]. In this process, large parallel sheets of PI films are laser scribed simultaneously, as demonstrated in Figure S1 (Supporting Information). LSG powder scratched from LSG film was further rolled to a free-standing LSG interlayer film. The free-standing LSG interlayer is composed of 80% LSG powder, 10 % conductive acetylene black (CAB) and 10% binder (polytetrafluoroethylene, PTFE). A small amount of CAB was added to enhance the conductivity of the free-standing film, which in turn improves the efficiency of redox reaction and boosts the suppression of polysulfides shuttering [34]. In addition to enhancing the electronic conductivity LSG, the addition of CAB creates an optimal continuous interlayer that allows the electrons to pass through while suppressing polysulfides from immigration. The free-standing LSG, with a thickness of about 90 μm, was painlessly intercalated between the cathode and the separator, as shown in Figure 1.

LSG powder was characterized by several physical characterization techniques, as demonstrated in Figure 2. The X-ray diffraction (XRD) pattern (Figure 2a) shows an intense asymmetric peak located at 2θ=25.9°, yielding an interlayer spacing of 3.4 Å between the (002) planes, which also confirms the high degree of graphitization of LSG. The interlayer spacing is attributed to regions of three-dimensional defective graphene layers. The peak at 2θ=42.9° is indexed to (100) plane. Furthermore, the Raman spectrum of LSG (Figure 2b) shows three peaks:

the D peak at 1,350 cm^{-1} imposed by bent sp^2-carbon bonds, the G peak at 1,580 cm^{-1} and the 2D peak at 2,700 cm^{-1}, both of which are fitted to the randomly stacked layers of graphene. More importantly, the intensity ratio of the 2D and G peaks confirms a high-quality formation of multilayered graphene [35].

The specific surface area and pore size distribution of LSG powder were evaluated by N_2 adsorption-desorption analysis. The isotherm of LSG is a combined I/IV type according to the International Union of Pure and Applied Chemistry (IUPAC) classification of isotherms, which indicates the existence of mesopores, micropores and macropores in the graphene structure, as illustrated in Figure 2c and Figure 2d. The pore size distribution curve of LSG shows micropores of less than 2 nm (red background), mesopores between 2 nm to 50 nm (yellow background) and macropores larger than 50 nm (blue background). The hierarchical porosity of LSG gives a unique permeable structure where nanosized pores act as active barrier sites for polysulfides while the larger pores facilitate electrolyte diffusion. [11,36] Additionally, the Brunauer–Emmett–Teller (BET) model was utilized to calculate the specific surface area of LSG (206.7 m^2 g^{-1}). The distinctive hierarchical morphology and the large surface area of LSG powder allow for the integration of CAB particles, forming a well-defined free-standing hybrid film.

The scanning electron microscopy (SEM) and transmission electron microscopy (TEM) images and the in Figure 2e and Figure 2f indicate the three-dimensionality with various levels of porosity in LSG powder. The analysis of the high-resolution TEM images (Figure 2g and Figure 2h) gives a d-spacing of 3.4 Å, with a range of 4 to 8 stacked layers. These findings are in good agreement with the data acquired by XRD. Additional SEM images of LSG powder and the free-standing LSG interlayer at different scales are supplemented in the supporting information (Figure S2), which beautifully shows their unique hierarchical structure.

To explore the practical applications of our LSG free-standing interlayer, we examined a Li-S battery with the free-standing LSG interlayer compared with a Li-S battery constructed without an interlayer. Li-S battery with LSG interlayer shows a profoundly enhanced cycling performance compared to the pristine Li-S battery, as demonstrated in Figure 3a. With the LSG interlayer, the Li-S cell exhibits an initial discharge capacity of 1165 mAh g^{-1} and maintains a high reversible capacity of 938 mAh g^{-1} at the current density of 0.25C after 100 cycles (assuming 1C = 1675 mA g^{-1}). It is worthwhile to note that the LSG interlayer enabled excellent capacity retention of 80.4%, which is among the highest values reported in the literature (see Table S1 in the Supporting Information). Even at a higher current density of 1C, the Li-S battery with LSG interlayer gives a high initial discharge capacity of 1022 mAh g^{-1} and retains a reversible capacity of ~750 mAh g^{-1} after 100 cycles. Furthermore, the battery with LSG interlayer showed an excellent rate capability when tested at high current densities. Figure 3b shows the rate performance of the Li-S battery with and without LSG at different current densities from 0.25C to 6C. The first three-cycle galvanostatic charge/discharge profiles of the cell with LSG confirms the reversibility and stability of the battery. The permanent capacity loss at the first cycle can be attributed to the formation of solid electrolyte interphase (SEI) [37].

The slopes of the charge-discharge curves correlate well with the cyclic voltammetry (CV) curves, as shown in Figure 3c, 3d, and Figure S3. The CV curves show a one anodic split doublet between 2.3 and 2.5 V and two cathodic peaks (2.05 V and 2.3–2.35 V), as typically observed in Li-S batteries. In the first three CV cycles, the locations of the anodic and cathodic peaks hardly change, indicating excellent electrochemical stability of the battery system. Besides, the diffusion coefficient of as-assembled batteries was calculated from CV measurement using Randles-Sevcik equation.[38]

$$i_p = 0.4463nFAC(\frac{nF\upsilon D}{RT})^{\frac{1}{2}}$$

Where i_p is the peak current (A), n is number of electrons transferred during the redox process (here, n=2), F is Faraday constant (C mol^{-1}). A is the contact area between sulfur cathode and electrolyte (here the geometric area of electrode is 1.13 cm^2), C is the bulk concentration of lithium in electrode (0.54 mmol cm^{-3}), D is diffusion coefficient (cm^2 s^{-1}), R is gas constant (J K^{-1} mol^{-1}), T is absolute temperature (K) and v is the scan rate. The Li^+ diffusion co-efficient of Li-Sulfur battery during discharge from 1.9-2.1 V is 4.65 × 10^{-7} cm^2 s^{-1}, while the Li^+ diffusion coefficient of Li-Sulfur battery with LSG interlayer is 4.77 × 10^{-6} cm^2 s^{-1}. The Li^+ diffusion coefficient with LSG free-standing film is obviously higher than Li-S battery without LSG interlayer, which shows the same tendency with the previously reported result.[39] This is ascribed to the enlarged electrochemical active surface area due to the addition of LSG interlayer, which endows electron transfer on LSG, thus shortens the diffusion pathway.

To further investigate the influence of the free-standing LSG film on diffusion, Electrochemical Impedance Spectroscopy (EIS) measurements were carried out on two types of cells: a cell with LSG interlayer and a cell without LSG interlayer. Before cycling, the Nyquist plots (Figure 3f) of both cells are composed of one semicircle whose diameter represents charge transfer resistance R_{ct} and a slope line corresponding to Warburg diffusion impedance. The cell with LSG interlayer yields a lower value of R_{ct} than the cell without an LSG interlayer, demonstrating enhanced ionic conductivity at the electrode/electrolyte interface in the LSG altered cells. After cycling, two semi-circles from high to middle frequency are observed (Figure 3g), which respectively correspond to interface contact impedance (high frequency, R_{sf}//LSG_{sf}) and charge transfer impedance (middle frequency, R_{ct}//LSG_{dl})[40]. It can be easily noticed that the cell with LSG interlayer has a shallower second semi-circle, indicating that LSG is attributed to the enhancement of the transformation between sulfur and polysulfides. Figure 3h shows the decrease

of both contact resistance and charge transfer resistance with cycling, confirming the ability of LSG interlayer to act as a conductive shell enhancing electron transfer and a shield suppressing the shuttling effect.

Besides electrochemical assessment, the ability of LSG interlayers to suppress polysulfide shuttling was examined qualitatively by the filtering experiment and quantitatively by the steady-state current shuttling measurements. Figure 4a shows that polysulfides diffused instantly through the glass fiber, a commonly used separator, while they were still well confined by the free-standing LSG interlayer even after 4 hours. A similar trend was observed when two cells, one with LSG and one without, were let to reach equilibrium after being cycled three times and held at constant discharge depth of 2 V.[41] Figure 4b indicates that a Li-S cell with LSG interlayer takes twice as long to reach equilibrium than the one without LSG. These results prove the superior confining ability of LSG to polysulfide migration.

Furthermore, Energy-dispersive X-ray spectroscopy (EDS) mapping of washed LSG interlayer after being run for 250 cycles was conducted to determine whether there was any chemical adsorption of polysulfides. The EDS findings revealed 5.4 wt.% of S, distributed evenly in the LSG interlayer, as demonstrated in Figure 4c, which indicates the chemical confinement of polysulfides in the free-standing LSG film.

In order to reveal the bonding environment of LSG interlayer, same sized samples of LSG interlayers were examined by an X-ray Photoelectron Spectroscopy (XPS) before cycling, after 100 cycles, and after 250 cycles (survey spectra is shown in Figure S4). The detected peaks show a general trend of increased bond formation of Li 1s and S 2p with cycling, as presented in Figure 4d and Figure 4e. The Li 1s XPS spectra after cycling show one dominant peak at 55.9 eV attributed to $LiSO_4$ while no peak exists in the uncycled interlayer. To obtain further insights, the

XPS of S 2p after 100 cycles (Figure. 4f) were analyzed and fitted into three different functional groups: $LiSO_4$ sulfate at 169.05 eV, SO_2-C sulfone at 167.5 eV, and C-S-C bonds at 163.6 eV. For the 250 cycles, an additional functional group appeared, $(S_2)^{-2}$ disulfide at 162.3 eV. The existence and enhanced signal of C-S-C indicate that LSG shows good chemical adsorption towards polysulfides. [40–42] The existence of such functional groups, namely sulfates, confirms that LSG interlayer undergoes chemical adsorption of polysulfides.

3. CONCLUSIONS

We have designed a straightforward method of fabricating a free-standing LSG film to suppress polysulfide shuttling in Li-S batteries by both physisorption and chemical adsorption. The distinctive morphology of the free-standing LSG interlayers with hierarchical three-dimensional pores hosting nanosized carbon particles enabled Li-S batteries to exhibit excellent electrochemical performance. A Li-S cell intercalated with the free-standing LSG film delivered a high specific capacity of 1160 mAh g^{-1} at 0.25C with an excellent capacity retention of 80.4% after 100 cycles, which is among the highest previously reported retention capabilities for Li-S batteries with carbonaceous interlayers (Supporting Information, Table S1).

4. Experimental Section

4.1 Materials Preparation

To synthesize LSG film, a laser power of 3.4 W was performed on a commercial Kapton PI (125 μm thickness, Dasom RMS Co. LTD,) sheet by Universal X-660 laser cutter platform (ULS PLS6.75, laser peak power 75 W). The wavelength is 10.6 μm and the pulse duration is around 14 μs. The pulses per inch (PPI) and the image quality level were set at 1000 and. The Z-distance between the laser and the sample was optimized to be 0.5 mm above the surface. The beam size was roughly around 100 μm. Then, the powder of LSG was obtained by scratching the

LSG film by a sharp edge. To make a free-standing LSG film with a thickness of about 90 μm, 80% LSG, 10 % conductive acetylene black and 10% binder (polytetrafluoroethylene, PTFE) were mixed in ethanol. After the ethanol had evaporated under 90 ^{o}C, the mixture was rolled on a glass substrate using a glass tube. The LSG films were cut into interlayer discs of 16 mm in diameter and dried in a vacuum glass tube oven for 2 hours.

4.2 Material Characterization

The material structure was characterized by X-ray diffraction (XRD) by a Bruker diffractometer (D8 Series II Advance) using Cu K (λ = 1.5406 Å) radiation. Raman spectra were recorded using Horiba LabRAM HR spectrometer with He-Ne laser at 633 nm. XPS studies were performed with a Kratos AXIS Ultra DVD (Kratos Analytical Ltd) at a base pressure of 1×10^{-9} Torr with a monochromatic Al Kα X-ray source operating at 150 W. Before the measurements, the samples were washed with DME solvent to ensure the removal of any physical attachment of polysulfides. The imaging of LSG morphology and the elemental EDS study were conducted using a scanning electron microscope (SEM) (model: Merlin, Carl Zeiss microscope Germany), and High-resolution transmission electron microscope (HRTEM) using FEI Titan 80–300 kV microscope.

4.3 Electrochemical Measurements

The sulfur cathode was prepared by the same process reported in Kim's group.[43] The sulfur content was ~2 mg cm^{-2}. For the measurement of electrochemical performance, 2032 coin cells (MTI, Inc.) were assembled in an Ar-filled glove box (H_2O and O_2 < 0.5 ppm). Pure Li metal foil, GC-50 glass fiber (Advantec) and 1.0 M lithium bis-trifluoromethane sulfonylimide (LiTFSI, Sigma-Aldrich) in 1,3-dioxolane (DOL, Sigma-Aldrich) and 1,2-dimethoxyethane (DME, Sigma-Aldrich) at a volume ratio of 1:1 with 0.4 M lithium nitrate ($LiNO_3$, Sigma-Aldrich) additive were

used as a counter electrode, separator and electrolyte solution, respectively. To evaluate the polysulfide adsorption by the LSG interlayer, 0.5 M Li_2S_8 based-electrolyte solution was obtained by adding elemental S_8 and Li with a molar ratio of 1:2 in a prepared electrolyte, as provisory described. The mixture was stirred at 80 ^oC in an Ar-filled glove box overnight. Cyclic voltammetry (CV) was conducted on a VMP3 (Bio-logic, France) electrochemical workstation at the scan rate ranging from 0.05 to 0.1 mV s^{-1} in the potential range of 1.8–2.8 V (vs. Li/Li^+). Measurements of the polysulfide shuttling current were also performed on a VMP3 electrochemical workstation. After cycling for three times, cells were discharged to 2 V and were allowed to equilibrate under a constant voltage to measure the study state current. Galvanostatic discharge and charge at different current densities were measured by an Arbin BT-2043 battery testing system in the potential range of 1.8–2.8 V (vs. Li/Li^+). EIS measurements were carried out by applying a sinusoidal wave with an amplitude of 5.0 mV over the frequency range from 100 kHz to 0.01 Hz at open-circuit voltage.

ASSOCIATED CONTENT

Supporting Information

Supplementary data associated with this article can be found in the online version at:

Details about how to prepare the LSG; SEM images of LSG powder and the free-standing LSG film at different scales, XPS complete analysis of samples; CV data for the pristine cell after cycling; and a comparison between different carbon-based interlayers in Li-S batteries are provided in the supporting information.

AUTHOR INFORMATION

Corresponding Author

*E-mail: husam.alshareef@kaust.edu.sa (Husam N. Alshareef)

Acknowledgments

This work was funded by the King Abdullah University of Science and Technology (KAUST), Kingdom of Saudi Arabia. The schematic illustration, in Figure 1 as well as in the Table of Contents Graphic, was implemented by Ebtehal Alzuwaid.

References

(1) Newbery, D. Shifting Demand and Supply over Time and Space to Manage Intermittent Generation: The Economics of Electrical Storage. *Energy Policy* **2018**, *113*, 711–720. https://doi.org/10.1016/J.ENPOL.2017.11.044.

(2) Scrosati, B.; Garche, J. Lithium Batteries: Status, Prospects and Future. *J. Power Sources* **2010**, *195* (9), 2419–2430. https://doi.org/10.1016/J.JPOWSOUR.2009.11.048.

(3) Fang, R.; Zhao, S.; Sun, Z.; Wang, D. W.; Cheng, H. M.; Li, F. More Reliable Lithium-Sulfur Batteries: Status, Solutions and Prospects. *Advanced Materials*. Wiley-VCH Verlag December 27, 2017, p 1606823. https://doi.org/10.1002/adma.201606823.

(4) Larcher, D.; Tarascon, J.-M. Towards Greener and More Sustainable Batteries for Electrical Energy Storage. *Nat. Chem.* **2015**, *7* (1), 19–29. https://doi.org/10.1038/nchem.2085.

(5) Bruce, P. G.; Freunberger, S. A.; Hardwick, L. J.; Tarascon, J.-M. Li–O2 and Li–S Batteries with High Energy Storage. *Nat. Mater.* **2012**, *11* (1), 19–29. https://doi.org/10.1038/nmat3191.

(6) Peng, H.-J.; Huang, J.-Q.; Cheng, X.-B.; Zhang, Q. Review on High-Loading and High-Energy Lithium-Sulfur Batteries. *Adv. Energy Mater.* **2017**, *7* (24), 1700260. https://doi.org/10.1002/aenm.201700260.

(7) Ji, X.; Nazar, L. F. Advances in Li–S Batteries. *J. Mater. Chem.* **2010**, *20* (44), 9821. https://doi.org/10.1039/b925751a.

(8) Chen, X.; Hou, T.; Persson, K. A.; Zhang, Q. Combining Theory and Experiment in Lithium–Sulfur Batteries: Current Progress and Future Perspectives. *Mater. Today* **2019**, *22*, 142–158. https://doi.org/10.1016/J.MATTOD.2018.04.007.

(9) Yan, M.; Wang, W.-P.; Yin, Y.-X.; Wan, L.-J.; Guo, Y.-G. Interfacial Design for Lithium–Sulfur Batteries: From Liquid to Solid. *EnergyChem* **2019**, *1* (1), 100002. https://doi.org/10.1016/J.ENCHEM.2019.100002.

(10) Mikhaylik, Y. V.; Akridge, J. R. Polysulfide Shuttle Study in the Li/S Battery System. *J. Electrochem. Soc.* **2004**, *151* (11), A1969. https://doi.org/10.1149/1.1806394.

(11) Qin, X.; Wu, J.; Xu, Z.-L.; Chong, W. G.; Huang, J.-Q.; Liang, G.; Li, B.; Kang, F.; Kim, J.-K. Electrosprayed Multiscale Porous Carbon Microspheres as Sulfur Hosts for Long-Life Lithium-Sulfur Batteries. *Carbon N. Y.* **2019**, *141*, 16–24. https://doi.org/10.1016/J.CARBON.2018.09.048.

(12) Abdul Razzaq, A.; Yao, Y.; Shah, R.; Qi, P.; Miao, L.; Chen, M.; Zhao, X.; Peng, Y.; Deng, Z. High-Performance Lithium Sulfur Batteries Enabled by a Synergy between Sulfur and Carbon Nanotubes. *Energy Storage Mater.* **2019**, *16*, 194–202. https://doi.org/10.1016/J.ENSM.2018.05.006.

(13) Xu, J.; Zhang, W.; Chen, Y.; Fan, H.; Su, D.; Wang, G. MOF-Derived Porous N–Co_3O_4@N–C Nanododecahedra Wrapped with Reduced Graphene Oxide as a High Capacity Cathode for Lithium–Sulfur Batteries. *J. Mater. Chem. A* **2018**, *6* (6), 2797–2807. https://doi.org/10.1039/C7TA10272K.

(14) Su, Y.-S.; Manthiram, A. Lithium–Sulphur Batteries with a Microporous Carbon Paper as a Bifunctional Interlayer. *Nat. Commun.* **2012**, *3* (1), 1166.

https://doi.org/10.1038/ncomms2163.

(15) Fan, L.; Li, M.; Li, X.; Xiao, W.; Chen, Z.; Lu, J. Interlayer Material Selection for Lithium-Sulfur Batteries. *Joule* **2019**, *3* (2), 361–386. https://doi.org/10.1016/j.joule.2019.01.003.

(16) Li, M.; Wan, Y.; Huang, J. K.; Assen, A. H.; Hsiung, C. E.; Jiang, H.; Han, Y.; Eddaoudi, M.; Lai, Z.; Ming, J.; et al. Metal-Organic Framework-Based Separators for Enhancing Li-S Battery Stability: Mechanism of Mitigating Polysulfide Diffusion. *ACS Energy Lett.* **2017**, *2* (10), 2362–2367. https://doi.org/10.1021/acsenergylett.7b00692.

(17) Chung, S.-H.; Manthiram, A. A Natural Carbonized Leaf as Polysulfide Diffusion Inhibitor for High-Performance Lithium-Sulfur Battery Cells. *ChemSusChem* **2014**, *7* (6), 1655–1661. https://doi.org/10.1002/cssc.201301287.

(18) Yang, K.; Zhong, L.; Guan, R.; Xiao, M.; Han, D.; Wang, S.; Meng, Y. Carbon Felt Interlayer Derived from Rice Paper and Its Synergistic Encapsulation of Polysulfides for Lithium-Sulfur Batteries. *Appl. Surf. Sci.* **2018**, *441*, 914–922. https://doi.org/10.1016/J.APSUSC.2018.02.108.

(19) Zhao, Q.; Zhu, Q.; An, Y.; Chen, R.; Sun, N.; Wu, F.; Xu, B. A 3D Conductive Carbon Interlayer with Ultrahigh Adsorption Capability for Lithium-Sulfur Batteries. *Appl. Surf. Sci.* **2018**, *440*, 770–777. https://doi.org/10.1016/J.APSUSC.2018.01.162.

(20) Zhang, L.; Wan, F.; Wang, X.; Cao, H.; Dai, X.; Niu, Z.; Wang, Y.; Chen, J. Dual-Functional Graphene Carbon as Polysulfide Trapper for High-Performance Lithium Sulfur Batteries. *ACS Appl. Mater. Interfaces* **2018**, *10* (6), 5594–5602. https://doi.org/10.1021/acsami.7b18894.

(21) Du, Z.; Guo, C.; Wang, L.; Hu, A.; Jin, S.; Zhang, T.; Jin, H.; Qi, Z.; Xin, S.; Kong, X.; et al. Atom-Thick Interlayer Made of CVD-Grown Graphene Film on Separator for Advanced Lithium–Sulfur Batteries. *ACS Appl. Mater. Interfaces* **2017**, *9* (50), 43696–43703. https://doi.org/10.1021/acsami.7b14195.

(22) Wang, X.; Wang, Z.; Chen, L. Reduced Graphene Oxide Film as a Shuttle-Inhibiting Interlayer in a Lithium–Sulfur Battery. *J. Power Sources* **2013**, *242*, 65–69. https://doi.org/10.1016/j.jpowsour.2013.05.063.

(23) Chai, L.; Wang, J.; Wang, H.; Zhang, L.; Yu, W.; Mai, L. Porous Carbonized Graphene-Embedded Fungus Film as an Interlayer for Superior Li–S Batteries. *Nano Energy* **2015**, *17*, 224–232. https://doi.org/10.1016/J.NANOEN.2015.09.001.

(24) Wang, L.; Yang, Z.; Nie, H.; Gu, C.; Hua, W.; Xu, X.; Chen, X.; Chen, Y.; Huang, S. A Lightweight Multifunctional Interlayer of Sulfur–Nitrogen Dual-Doped Graphene for Ultrafast, Long-Life Lithium–Sulfur Batteries. *J. Mater. Chem. A* **2016**, *4* (40), 15343–15352. https://doi.org/10.1039/C6TA07027B.

(25) Gu, X.; Tong, C. J.; Lai, C.; Qiu, J.; Huang, X.; Yang, W.; Wen, B.; Liu, L. M.; Hou, Y.; Zhang, S. A Porous Nitrogen and Phosphorous Dual Doped Graphene Blocking Layer for High Performance Li-S Batteries. *J. Mater. Chem. A* **2015**, *3* (32), 16670–16678. https://doi.org/10.1039/c5ta04255k.

(26) Liu, Y.; Qin, X.; Zhang, S.; Liang, G.; Kang, F.; Chen, G.; Li, B. Fe_3O_4 -Decorated Porous Graphene Interlayer for High-Performance Lithium–Sulfur Batteries. *ACS Appl. Mater. Interfaces* **2018**, *10* (31), 26264–26273. https://doi.org/10.1021/acsami.8b07316.

(27) Alam, S. N.; Sharma, N.; Kumar, L. Synthesis of Graphene Oxide (GO) by Modified

Hummers Method and Its Thermal Reduction to Obtain Reduced Graphene Oxide (RGO)*. *Graphene* **2017**, *06* (01), 1–18. https://doi.org/10.4236/graphene.2017.61001.

(28) Ye, R.; James, D. K.; Tour, J. M. Laser-Induced Graphene: From Discovery to Translation. *Adv. Mater.* **2018**, 1803621. https://doi.org/10.1002/adma.201803621.

(29) Xu, G.; Jarjes, Z. A.; Desprez, V.; Kilmartin, P. A.; Travas-Sejdic, J. Sensitive, Selective, Disposable Electrochemical Dopamine Sensor Based on PEDOT-Modified Laser Scribed Graphene. *Biosens. Bioelectron.* **2018**, *107*, 184–191. https://doi.org/10.1016/j.bios.2018.02.031.

(30) Zhang, W.; Lei, Y.; Ming, F.; Jiang, Q.; Costa, P. M. F. J.; Alshareef, H. N. Lignin Laser Lithography: A Direct-Write Method for Fabricating 3D Graphene Electrodes for Microsupercapacitors. *Adv. Energy Mater.* **2018**, *8* (27), 1801840. https://doi.org/10.1002/aenm.201801840.

(31) Zhang, F.; Alhajji, E.; Lei, Y.; Kurra, N.; Alshareef, H. N. Highly Doped 3D Graphene Na-Ion Battery Anode by Laser Scribing Polyimide Films in Nitrogen Ambient. *Adv. Energy Mater.* **2018**, *8* (23). https://doi.org/10.1002/aenm.201800353.

(32) Kurra, N.; Jiang, Q.; Nayak, P.; Alshareef, H. N. Laser-Derived Graphene: A Three-Dimensional Printed Graphene Electrode and Its Emerging Applications. *Nano Today*. Elsevier February 1, 2019, pp 81–102. https://doi.org/10.1016/j.nantod.2018.12.003.

(33) Lin, J.; Peng, Z.; Liu, Y.; Ruiz-Zepeda, F.; Ye, R.; Samuel, E. L. G.; Yacaman, M. J.; Yakobson, B. I.; Tour, J. M. Laser-Induced Porous Graphene Films from Commercial Polymers. *Nat. Commun.* **2014**, *5* (1), 5714. https://doi.org/10.1038/ncomms6714.

(34) Zhang, B.; Lai, C.; Zhou, Z.; Gao, X. P. Preparation and Electrochemical Properties of Sulfur–Acetylene Black Composites as Cathode Materials. *Electrochim. Acta* **2009**, *54* (14), 3708–3713. https://doi.org/10.1016/J.ELECTACTA.2009.01.056.

(35) Ferrari, A. C.; Meyer, J. C.; Scardaci, V.; Casiraghi, C.; Lazzeri, M.; Mauri, F.; Piscanec, S.; Jiang, D.; Novoselov, K. S.; Roth, S.; et al. Raman Spectrum of Graphene and Graphene Layers. *Phys. Rev. Lett.* **2006**, *97* (18). https://doi.org/10.1103/PhysRevLett.97.187401.

(36) Balach, J.; Jaumann, T.; Klose, M.; Oswald, S.; Eckert, J.; Giebeler, L. Functional Mesoporous Carbon-Coated Separator for Long-Life, High-Energy Lithium-Sulfur Batteries. *Adv. Funct. Mater.* **2015**, *25* (33), 5285–5291. https://doi.org/10.1002/adfm.201502251.

(37) Xiong, S.; Xie, K.; Diao, Y.; Hong, X. Characterization of the Solid Electrolyte Interphase on Lithium Anode for Preventing the Shuttle Mechanism in Lithium–Sulfur Batteries. *J. Power Sources* **2014**, *246*, 840–845. https://doi.org/10.1016/J.JPOWSOUR.2013.08.041.

(38) Steimecke, M.; Rümmler, S.; Bron, M. The Effect of Rapid Functionalization on the Structural and Electrochemical Properties of High-Purity Carbon Nanotubes. *Electrochim. Acta* **2015**, *163*, 1–8. https://doi.org/10.1016/j.electacta.2015.02.142.

(39) Enhanced Cycling Performance for Lithium–Sulfur Batteries by a Laminated 2D g-C3N4/Graphene Cathode Interlayer - Qu - 2019 - ChemSusChem - Wiley Online Library https://onlinelibrary.wiley.com/doi/full/10.1002/cssc.201802449 (accessed Mar 4, 2020).

(40) Kong, W.; Yan, L.; Luo, Y.; Wang, D.; Jiang, K.; Li, Q.; Fan, S.; Wang, J. Ultrathin

MnO2/Graphene Oxide/Carbon Nanotube Interlayer as Efficient Polysulfide-Trapping Shield for High-Performance Li–S Batteries. *Adv. Funct. Mater.* **2017**, *27* (18). https://doi.org/10.1002/adfm.201606663.

(41) Moy, D.; Manivannan, A.; Narayanan, S. R. Direct Measurement of Polysulfide Shuttle Current: A Window into Understanding the Performance of Lithium-Sulfur Cells. *J. Electrochem. Soc.* **2015**, *162* (1), A1–A7. https://doi.org/10.1149/2.0181501jes.

(42) Etacheri, V.; Marom, R.; Elazari, R.; Salitra, G.; Aurbach, D. Challenges in the Development of Advanced Li-Ion Batteries: A Review. *Energy Environ. Sci.* **2011**, *4* (9), 3243. https://doi.org/10.1039/c1ee01598b.

(43) Huang, J. Q.; Xu, Z. L.; Abouali, S.; Akbari Garakani, M.; Kim, J. K. Porous Graphene Oxide/Carbon Nanotube Hybrid Films as Interlayer for Lithium-Sulfur Batteries. *Carbon N. Y.* **2016**, *99*, 624–632. https://doi.org/10.1016/j.carbon.2015.12.081.

Figures:

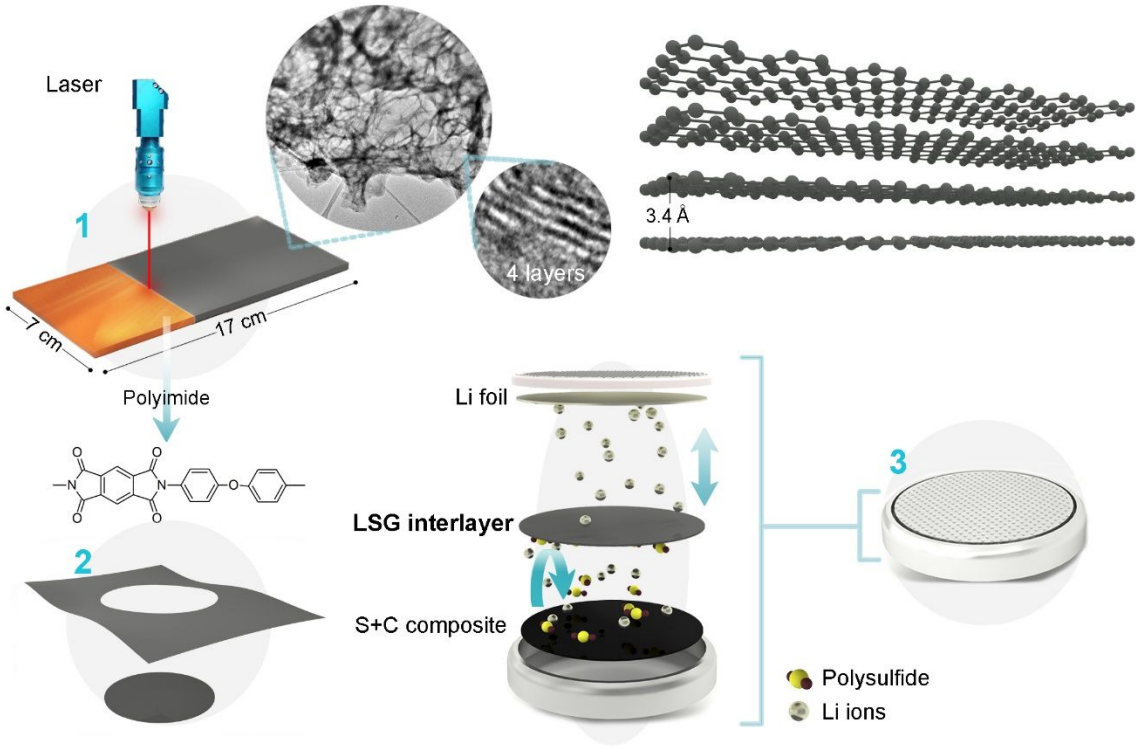

Figure 1. Schematic illustration of the synthetic process of the free-standing LSG interlayer for Li-S battery. Graphic design implemented by Ebtehal Alzuwaid.

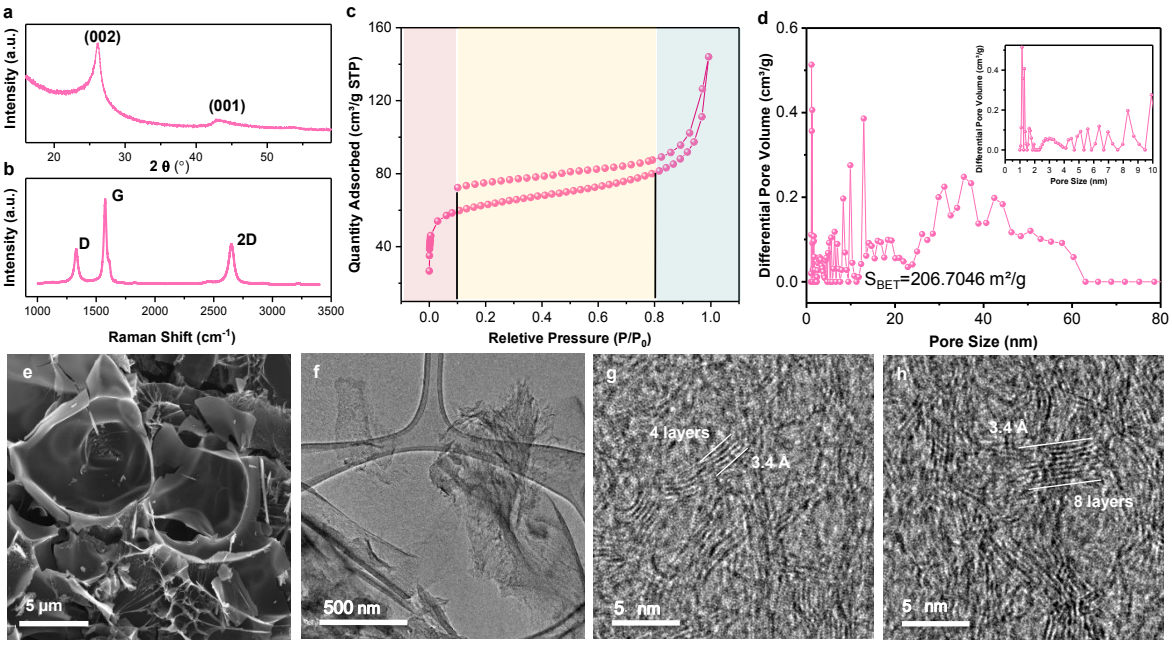

Figure 2. Physicochemical characterization of LSG: (a) XRD pattern; (b) Raman spectrum; (c) N_2 adsorption-desorption isotherm curve and (d) pore size distribution curve; (e) SEM image; (f) TEM image (g) and (h) high resolution TEM images.

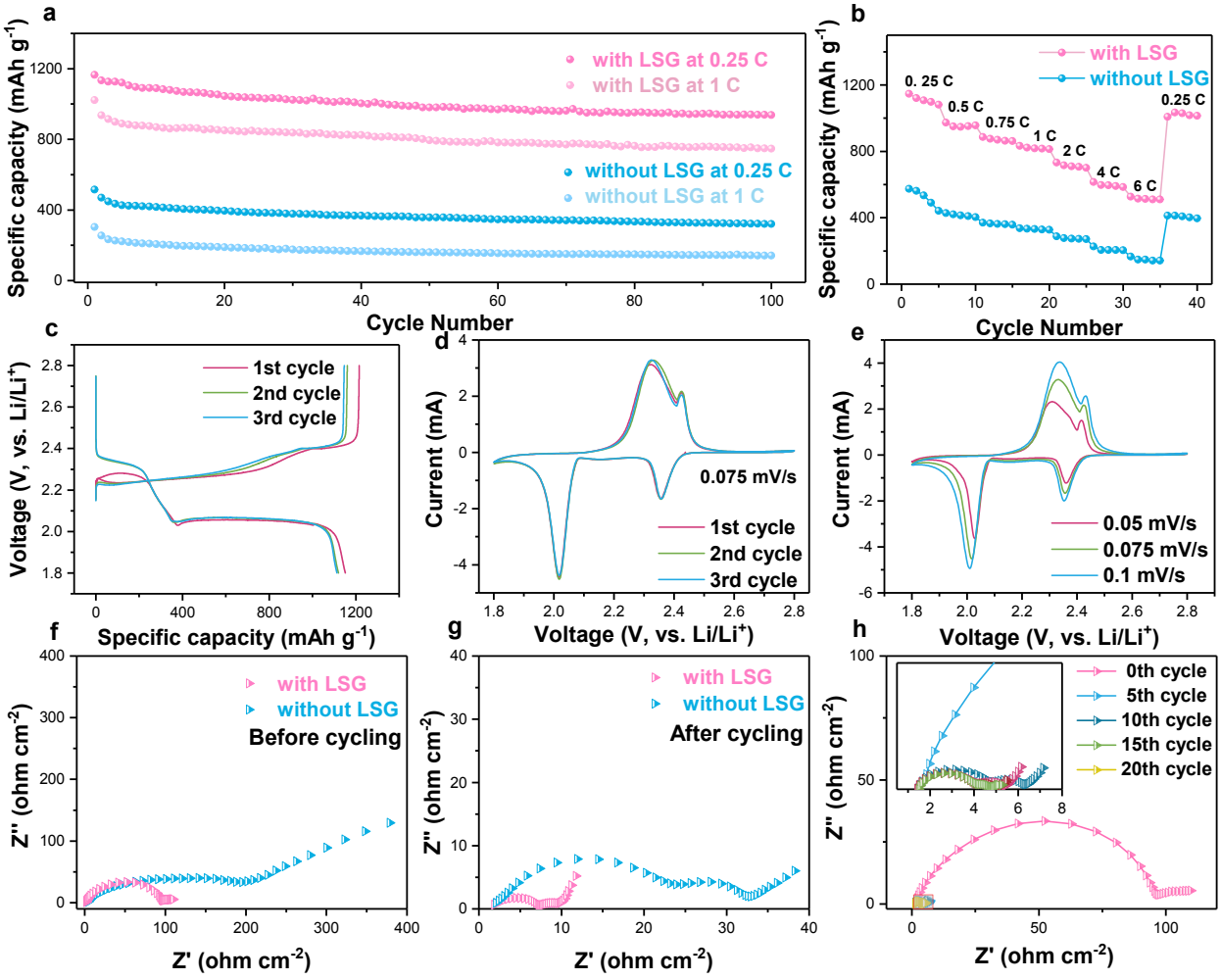

Figure 3. Electrochemical characterization: (a) cycling performances of Li-S cells with and without LSG interlayer at 0.25C and 1C for 100 cycles; (b) rate performance of Li-S cells with and without LSG interlayer at 0.25, 0.5, 0.75, 1, 2, 4, 6 and then back to 0.25C; (c) galvanostatic charge/discharge profiles of LSG interlayer in the 1st, 2nd, 3rd cycles at 0.25C, CV curves of LSG interlayer at (d) different cycles and (e) different scan rates; comparison of EIS data for cells with and without LSG interlayer (f) before cycling and (g) after cycling; (h) EIS plots of LSG interlayer modified Li-S battery after the 0th, 5th, 10th, 15th and 20th cycle.

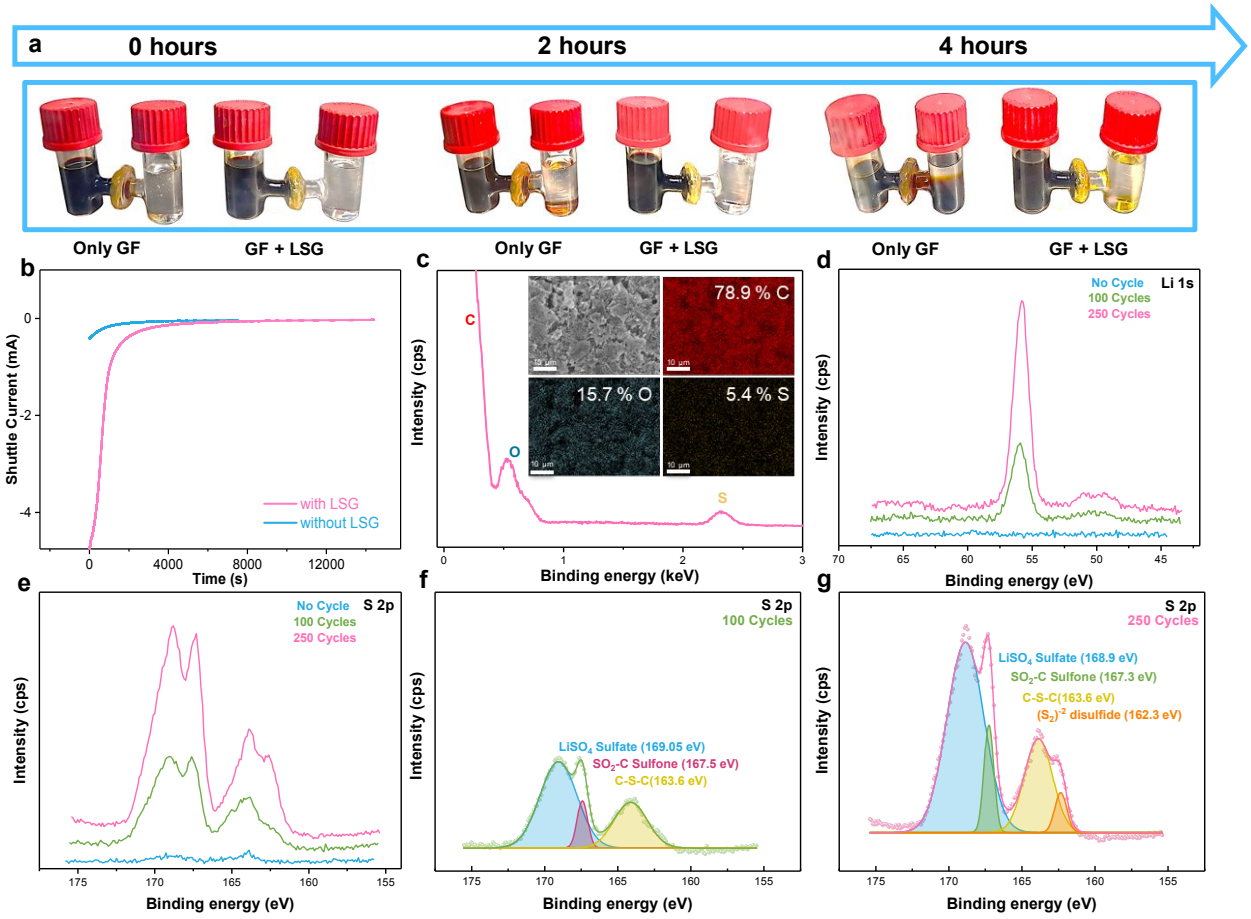

Figure 4. Shuttling prohibition characterization: (a) photographs of glass cells with polysulfides based electrolyte in one side and pure electrolyte in the other side after 0, 2 and 4 hours; (b) the steady-state shuttling current of Li-S battery with and without LSG (c) EDS mapping of washed LSG interlayer after 250 cycles; XPS spectra of LSG interlayer of (d) Li and (e) S after 0, 100 and 250 cycles, respectively; analyzed and fitted XPS spectra with functional groups of S 2p after (f) 100 and (g) 250 cycles.

Table Of Contents (TOC) graphic: